

Spin Dynamics and Light-Induced Effects in EuZn_2P_2

M. Dutra¹, G. G. Vasques¹, P. C. Sabino¹, J. G. Dias¹, J. F. Oliveira², M. A. A. Heringer², M. Cabrera-Baez³, E. Baggio Saitovitch², A. R. V. Benvenho¹, M. A. Avila¹, and J. Munevar^{1,4*}

¹*CCNH, Universidade Federal do ABC (UFABC), Santo Andre, SP, 09210-580, Brazil*

²*Centro Brasileiro de Pesquisas Físicas, Rua Doutor Xavier Sigaud 150, Rio de Janeiro, RJ, 22290-180, Brazil*

³*Departamento de Física, Universidade Federal de Pernambuco, Recife, PE, 50670-901, Brazil and*

⁴*Departamento de Física, Universidad del Valle, Cali, A. A. 25360, Colombia*

(Dated: June 10, 2025)

The magnetic spin dynamics and optical properties of EuZn_2P_2 are studied. Single crystals grown by the Sn-flux method crystallize in the $P\bar{3}m1$ (No. 164) space group and order antiferromagnetically at $T_N = 23.5$ K. ^{151}Eu Mössbauer spectroscopy confirms the presence of the Eu^{2+} oxidation state only and the magnetic moment angle relative to the c -axis is $\theta = 46(3)^\circ$. Temperature-dependent electron spin resonance (ESR) measurements reveal that spin-spin interactions predominantly govern the spin relaxation mechanisms, as evidenced by the linewidth behavior (ΔH). Positive g -shifts (Δg) for $H \parallel ab$ indicate the presence of local electron polarization. The ESR data support the formation of anisotropic magnetic polarons, which trap spin carriers and contribute to increased electrical resistance. Angular-dependent ESR spectra at room temperature display anisotropic behavior in both $\Delta g(\phi)$ and $\Delta H(\phi)$, with a dominant three-dimensional component C_{3D} , indicative of robust interlayer coupling and antiferromagnetic fluctuations. Under light illumination, a small broadening of ΔH is observed. Furthermore, a photovoltaic effect is identified in EuZn_2P_2 , with photodetector performance metrics suggesting promising capabilities for future optoelectronic devices.

I. INTRODUCTION

Zintl phases, conceptualized through the Zintl-Klemm framework, have garnered significant attention as prospective thermoelectric materials that offer environmentally friendly pathways for energy conversion [1]. This is in part due to the fact that many Zintl materials are known to have low environmental toxicity. These materials are characterized by the transfer of electrons from electropositive to electronegative elements, stabilizing polyanionic frameworks. One notable family within this class is represented by a subgroup of compounds with general formula RM_2X_2 : those where R is an alkali-earth or rare-earth element, M is a d^5 or d^{10} transition metal, and X is an element from groups 14 and 15 of the periodic table. They are stabilized by electron donation from the R element, thus satisfying the valence electron count required for structural integrity [2, 3]. Consequently, these compounds exhibit low electrical conductivity and are mainly semiconductors [4].

Eu-based compounds with the CaAl_2Si_2 -type structure, such as EuCd_2P_2 [5], EuCd_2As_2 [6], EuZn_2As_2 [7] exhibit colossal magnetoresistance (CMR) [5, 6, 8] and antiferromagnetic order at low temperatures. The observation of CMR in these materials is remarkable because it is usually observed in mixed-valence perovskites materials, which can exhibit ferromagnetism associated with double exchange or Jahn-Teller distortions

[9]. Various mechanisms have been proposed to explain the CMR behavior, such as electronic band reconstruction [10], spin-lattice coupling [11], and Berezinskii-Kosterlitz-Thouless (BKT) transitions [12], among others. These Eu-containing materials are also candidates for the realization of topological states. For instance, EuZn_2As_2 has been proposed to exhibit a topological phase transition under hydrostatic pressure [7]. Moreover, EuCd_2As_2 has shown evidence of multiple topological transitions, as supported by pressure-dependent measurements and density functional theory (DFT) calculations [8]. The interplay between magnetic and electronic degrees of freedom in these systems paves the way for novel quantum phenomena with potential applications in spintronics, quantum computing, and dark matter detection [13–16].

In addition to their magnetic and electronic properties, Zintl phases can also be promising optoelectronic materials; tuning the band gap of these materials can make them viable candidates for photovoltaic applications. Compounds such as SrCd_2X_2 ($\text{X} = \text{P}, \text{As}$) [17], BaCd_2P_2 [18], BaMg_2X_2 ($\text{X} = \text{P}, \text{As}, \text{Sb}$) [19], Ba_2ZnP_2 [20], and YbZn_2X_2 ($\text{X} = \text{P}, \text{As}, \text{Sb}, \text{Bi}$) [21] have demonstrated optoelectronic properties that are potentially suitable for solar energy conversion. However, to date, no photovoltaic effect has been reported in Eu-based CaAl_2Si_2 -type compounds in single-crystalline form. The intersection of magnetism and light-induced effects remains largely unexplored in intermetallics, primarily due to the intrinsic challenges in coupling light with magnetic properties. Photons do not interact directly with magnetic fields as electrons do, making such interactions difficult to probe and observe. Despite this, the unique potential of Eu-based CaAl_2Si_2 -type compounds indicate that

* Corresponding author: julian.munevar@correounivalle.edu.co;
Present address: Universidad del Valle, Cali, A. A. 25360, Colombia.

they may offer an ideal platform for studying the interplay between magnetism, optical excitation, and electronic behavior. When certain materials are exposed to illumination, electrons can undergo energy transitions. In such cases, photons absorbed by the electronic states can have a direct influence the magnetism. As the light is absorbed, it promotes the excitations of electrons into the conduction band or localized energy levels. In response, the electron density is redistributed and causes changes in the material magnetic properties [22, 23]. The photomagnetic effect can have relevant implications such as ultrafast control of magnetization [24], photomagnetic sensing with high sensitivity and low detection limits [25] and development of potential data storage devices with light-rewritable magnetic memory that does not require application of magnetic fields [26, 27].

In this work, we present experimental evidence of light-induced effects on the magnetism and spin dynamics of EuZn_2P_2 , as well as the discovery of a photovoltaic effect. These findings are supported by a combination of Mössbauer spectroscopy, ESR with and without light exposure, and room-temperature transport measurements under illumination.

II. METHODS

High-purity single crystals of EuZn_2P_2 were synthesized by the Sn-flux method. High purity elements, Eu (99.9%), Zn (99.999%), P (99.999%), and Sn (99.999%) from Alfa-Aesar, were weighted in an atomic ratio of 1:2:2:40 and placed inside a quartz tube with quartz wool. The evacuated and sealed ampoule was gradually heated to 500 °C over 2 h, maintained for 1 h, then further heated to 1150 °C over 4 h and held at this temperature for 10 h. Controlled cooling was carried out down to 850 °C at a rate of 2 °C/h, after which the tubes were rapidly spun to separate the crystals from the flux. The resulting single crystals were hexagonal in shape with approximately 1 mm x 1 mm x 0.5 mm. Powder X-ray diffraction (PXRD) was conducted at room temperature on crushed single crystals, using a Bruker D2 PHASER diffractometer with a LYNXEYE XE-T detector using $\text{Cu K}\alpha$ radiation with a wavelength of $\lambda_{\text{Cu}} = 1.5405 \text{ \AA}$.

Magnetic susceptibility measurements were carried out using a Quantum Design SQUID-MPMS3 system over the temperature range of 2-300 K. Measurements were taken with the external magnetic field applied parallel and perpendicular to the crystallographic c -axis using applied fields of 1 kOe, 10 kOe and 30 kOe. The electrical resistance was measured in a Quantum Design Dynacool cryostat, using the Electrical Transport Option (ETO) in high-impedance mode.

The ESR measurements were conducted using two setups: the temperature-dependent spectra were collected with a BRUKER - ELEXSYS 500 CW spectrometer equipped with a TE102 cavity operating at 9.4 GHz (X-band) using a continuous helium gas cryostat gas for tem-

peratures from 18 to 250 K. The sample was aligned with $H \parallel ab$ inside a quartz straw before being inserted in the cryostat. The magnetic field was swept from 1500 to 5500 Oe. Angular-dependent ESR measurements were performed on an ESR5000 spectrometer using 2 mW microwave power and external field sweep from 500 to 6000 Oe. The modulation frequency was set to 10 kHz. Direct optical stimulation was performed by using an integrated light source, operated through ESRStudio for fastest response times.

The $I - V$ curves were obtained using a Keithley 2602a source using different tensions with and without light. The potentials used for the photovoltaic effect measurements were 0.5 and 15 V using a light source of 1000 lumens. The transient curves were obtained using a laser with a wavelength of 686 nm.

III. RESULTS

A. Crystal Structure

The PXRD pattern and the Rietveld refinement obtained for the EuZn_2P_2 single crystals are shown in Fig. 1. Rietveld refinement was performed using the GSAS-II software [28], where a major phase was found corresponding to EuZn_2P_2 , that crystallizes in a trigonal crystal lattice belonging to the space group $P\bar{3}m1$ (No. 164), plus a minor phase corresponding to a small amount of elemental Sn. These Sn peaks are due to remaining flux on the EuZn_2P_2 crystal surface, which was mechanically removed prior to final crystal characterization.

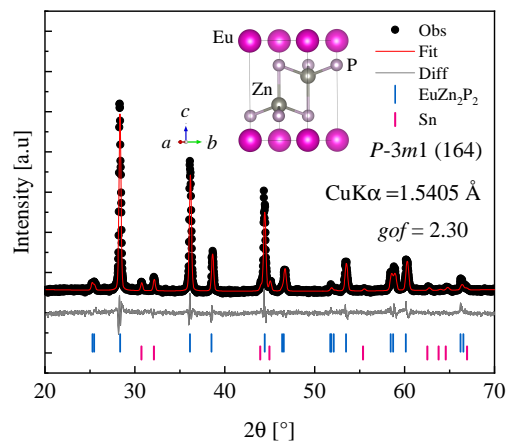


FIG. 1. X-ray diffraction pattern of EuZn_2P_2 . The experimental data is presented in black, the Rietveld refinement is shown in red, the difference between experiment and model is shown in gray, and the Bragg reflections corresponding to the Sn and EuZn_2P_2 are also shown as vertical lines. Inset are shown the EuZn_2P_2 unit cell.

The refined crystal structure (inset Fig. 1), consists of Eu^{2+} layers separated by $[\text{Zn}_2\text{P}_2]^{2-}$ clusters, consis-

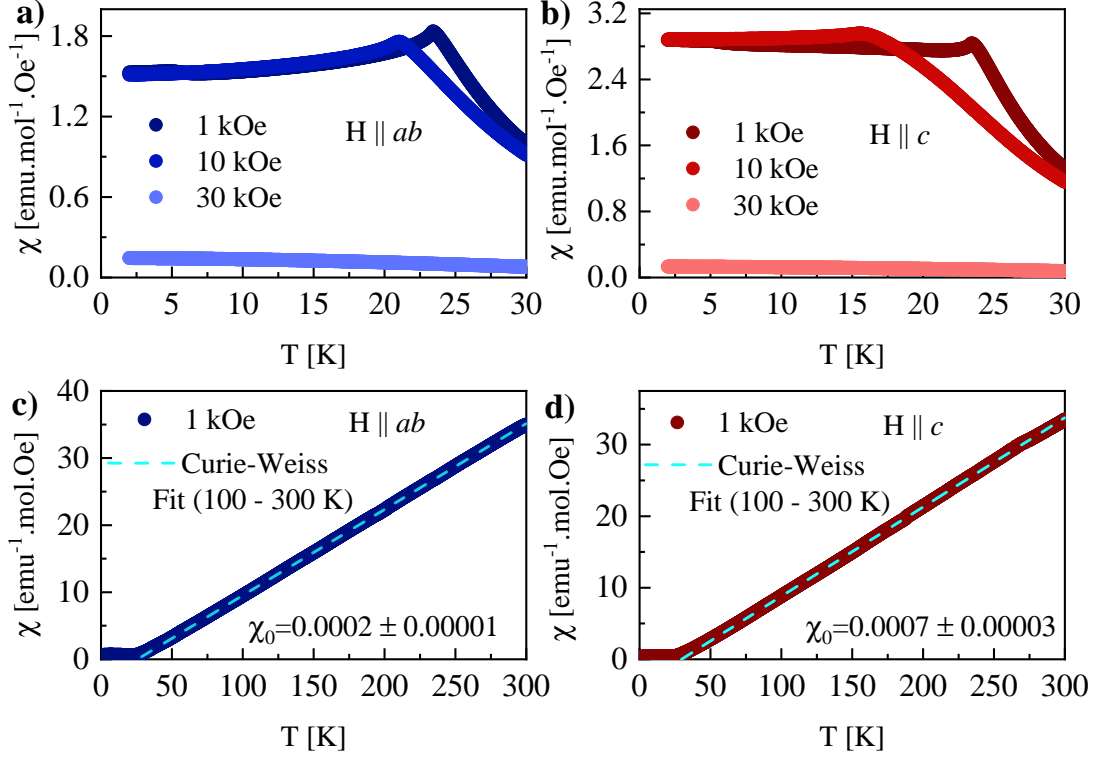


FIG. 2. a) Magnetic susceptibility $\chi(T)$ for EuZn_2P_2 for $H \parallel ab$ and $H \parallel c$. It is possible to visualize the AFM ordering near $T_N = 23.5$ K. As the applied field increase, the AFM order peak shifts to lower temperatures until its suppression. c) The Curie-Weiss analysis for $H \parallel ab$ and d) $H \parallel c$ on the χ^{-1} presenting linear behavior.

tent with the prototype structure CaAl_2Si_2 . The refined lattice parameters are $a = b = 4.0850(3)$ Å, and $c = 7.0029(3)$ Å, in good agreement with the literature [29].

B. Magnetic Susceptibility

Temperature-dependent magnetic susceptibility $\chi(T)$ was measured under various applied fields for both $H \parallel ab$ and $H \parallel c$ orientations (Fig. 2 (a-b)). An anti-ferromagnetic transition is observed at $T_N = 23.5$ K, which is suppressed upon increasing the magnetic field. The inverse susceptibility (χ^{-1}) data fit to the Curie-Weiss law between 100 and 300 K (Fig. 2 (c-d)) yield $\mu_{eff}^{H \parallel ab} = 7.85(9) \mu_B$ for $H \parallel ab$ and $\mu_{eff}^{H \parallel c} = 8.11(7)$ for $H \parallel c$, with corresponding Curie-Weiss temperatures of $\theta_{CW}^{H \parallel ab} = 28.1(7)$ K and $\theta_{CW}^{H \parallel c} = 27.9(8)$ K, respectively. These positive values of θ_{CW} suggest the predominance of short-range FM interactions between Eu^{2+} moments within each plane.

C. ^{151}Eu Mössbauer Spectroscopy

^{151}Eu Mössbauer spectra obtained at 300 K and 10 K for EuZn_2P_2 crushed single crystals are shown in Fig. 3.

Above T_N a single broad resonance line is observed, whereas below T_N the resonance line splits due to the onset of magnetic order. The spectra were fitted using the Full Hamiltonian site analysis for the ^{151}Eu nucleus, provided by the NORMOS software package.

The fitted parameters are the isomer shift δ , the quadrupole splitting ΔE_Q , the linewidth Γ , the magnetic hyperfine field B_{hf} , the resonance area and the angle θ between B_{hf} and the electric field gradient principal component V_{zz} , which has been taken parallel to the crystal c -axis.

At 300 K (Fig. 3a), a clear resonance line is obtained with a large negative isomer shift of $\delta = -11.1(9)$ mm/s, typical for Eu in the divalent state [30]. A small resonance asymmetry found in the spectrum at 300 K is attributed to the presence of a quadrupole splitting of $\Delta E_Q = 2.5(4)$ mm/s.

Since no structural phase transitions are known in this compound and since the Eu^{2+} has a half-filled $4f^7$ configuration, it is expected that the $4f$ electrons do not contribute to V_{zz} and thus the contribution to V_{zz} comes only from the crystal lattice. Therefore, this value of ΔE_Q will be used as an input for the low-temperature spectra fit. No clear evidence for Eu^{3+} or magnetic order are apparent in the 300 K spectrum.

The Mössbauer spectrum at 10 K (Fig. 3b) shows a resonance line splitting expected due to the onset of mag-

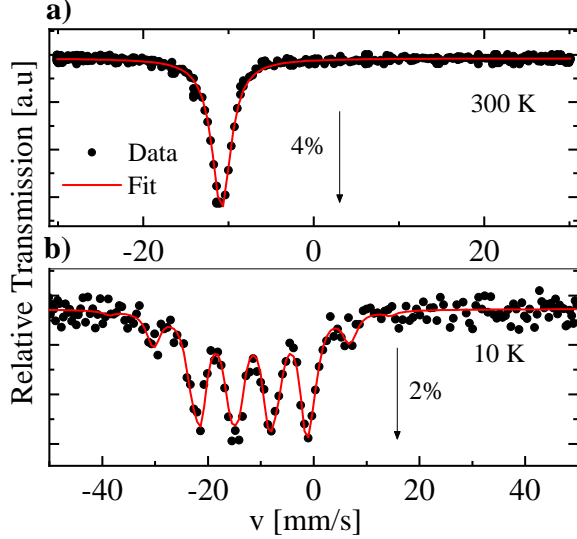


FIG. 3. a) Mössbauer spectra for EuZn_2P_2 at 300 K and the fitting (red line). The room temperature spectrum shows unique resonance line with negative velocities indicating the Eu^{2+} state. b) The 10 K spectrum present a series of resonance line related to the magnetic ordered state of Eu ion.

netic order of the Eu moments [31]. The magnetically split spectrum fit was performed taking the ΔE_Q value obtained at 300 K, and the resulting hyperfine parameters are $\delta = -11.4(1)$ mm/s, $B_{hf} = 25.2 \pm 0.1$ T, $\Gamma = 2.6(7)$ mm/s and $\theta = 46(3)^\circ$. Since $V_{zz} \parallel c$ is assumed, this means that the Eu moments are aligned at approximately 46° from the c -axis, which is consistent with previous reports [32].

D. Electron Spin Resonance

ESR measurements (Fig. 4a) were conducted on EuZn_2P_2 single crystals (18 - 250 K) with $H \parallel ab$. The ESR spectra reveal a single broad resonance line with small asymmetry and no hyperfine splitting, characteristic of localized magnetic moments in an exchanged-narrowed environment [33]. The spectra are well described by a Lorentzian admixture model combining absorption and dispersion components [34]:

$$\frac{d[(1-\alpha)\chi'' + \alpha\chi']}{dH} = \chi_0 H_0 \gamma_e^2 T_2^2 \left[\frac{2(1-\alpha)x}{(1+x^2)^2} + \frac{\alpha(1-x^2)}{(1+x^2)^2} \right], \quad (1)$$

where

$$x = (H_0 - H)\gamma_e^2 T_2, \quad (2)$$

H_0 and H are, respectively, the resonance and the external field, γ_e^2 is the ratio of the electron gyromagnetic factor, T_2 is the spin-spin relaxation time, α is the admixture of absorption ($\alpha = 0$) and dispersion ($\alpha = 1$) and χ_0

is the paramagnetic contribution from the static susceptibility. From these fits, the temperature evolution of the linewidth (ΔH) and g -shift (Δg) was extracted as shown in Fig. 4 (b-c). The $\Delta H(T)$ and $\Delta g(T)$ show exponential behavior, in good agreement with previous studies [35].

We use the same approach to obtain the $\Delta H(\phi)$ and $\Delta g(\phi)$ from ESR spectra at room temperature for different angles between the crystal and the magnetic field (Fig. 4d). The extracted $\Delta H(\phi)$ and $\Delta g(\phi)$ (Fig. 4e-f) display uniaxial behavior consistent with anisotropic magnetic interactions. The model used to fit the $\Delta g(\phi)$ data considers two components of the g -factor (g_{\parallel} and g_{\perp}) and is given by:

$$g(\phi) = \sqrt{g_{\parallel}^2 \cos^2 \phi + g_{\perp}^2 \sin^2 \phi}, \quad (3)$$

where ϕ is the angle between the external applied field and the c -axis. From the extracted components we note that $g_{\perp} > g_{\parallel}$, calculating the $\Delta g(\phi)$ yields both signs $\Delta g_{\perp}(\phi) > 0$ and $\Delta g_{\parallel}(\phi) < 0$. This anisotropic Eu^{2+} - Eu^{2+} magnetic coupling is consistent with the scenario revealed in magnetic susceptibility data, where short-range FM interactions are in the ab -plane and AFM interactions are between layers.

Another interesting observation arises from the analysis of the angular dependence of the linewidth, $\Delta H(\phi)$. The $\Delta H(\phi)$ data was extracted using models for 2D and 3D given by Eqs. 4 and 5:

$$\Delta H(\phi)_{3D} \propto C_{3D}(\cos^2(\phi) + 1), \quad (4)$$

$$\Delta H(\phi)_{2D} \propto C_{2D}(3\cos^2(\phi) - 1)^2, \quad (5)$$

where ϕ is the angle between the external magnetic field and the normal to the spin plane. Spin fluctuations yield dominant contributions from the C_{3D} , indicating three-dimensional, short-wavelength spin fluctuations with significant interplane coupling and AFM fluctuations character, in good agreement with previous studies [36].

E. Photoresponse

The photoresponse of EuZn_2P_2 was studied by analyzing the I - V characteristics and transient response curves shown in Fig. 5. The comparison of the I - V curves under dark and illuminated conditions at 0.5 V (Fig. 5a) reveals asymmetric and nonlinear behavior. Such characteristics are present in certain photodiodes [37]. The effect of light on the current is evident in Fig. 5c, as the photogenerated current can be switched on and off by toggling the light source.

When a bias voltage of 0.5 V is applied, the dark current (I_{Dark}) starts at approximately $0.56 \mu\text{A}$, which is relatively high even in the absence of illumination.

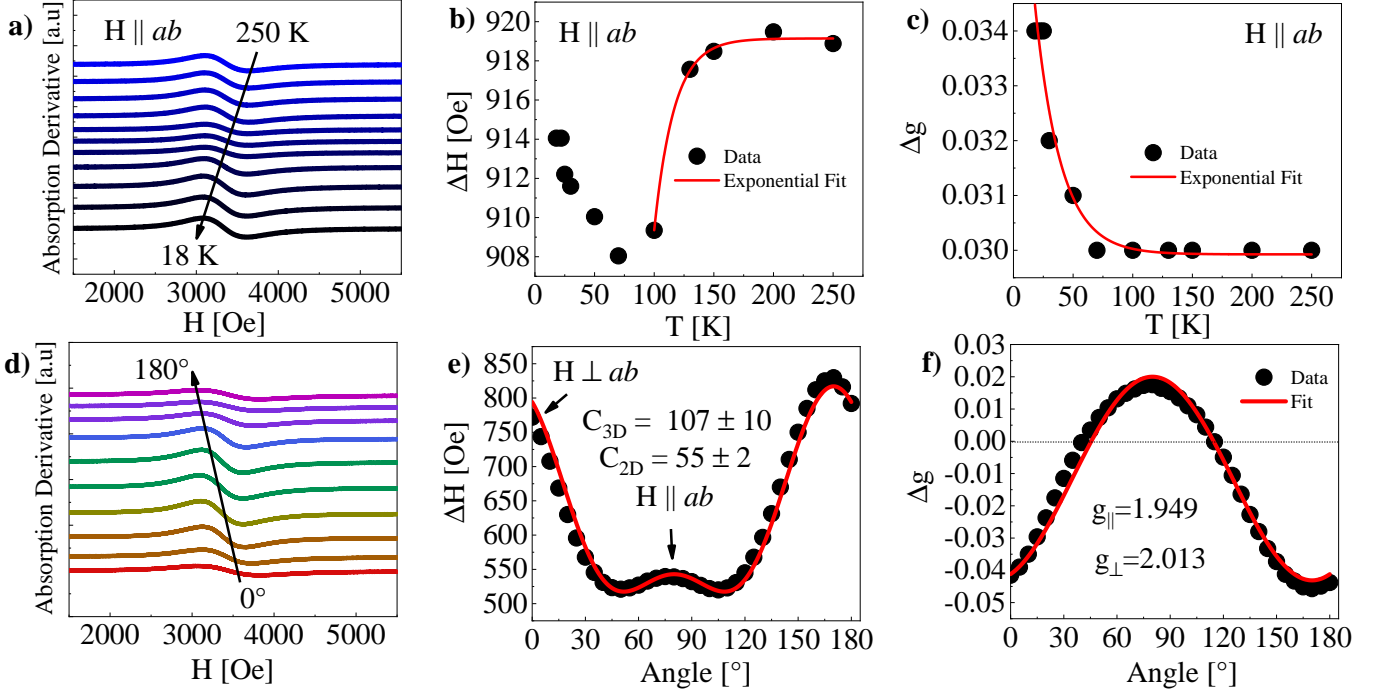


FIG. 4. a) Temperature-dependent ESR spectra for $H \parallel ab$ b) $\Delta H(T)$ and c) $\Delta g(T)$ extracted using equation 1. d) Angular-dependent ESR spectra at room-temperature e) $\Delta H(\phi)$ and f) $\Delta g(\phi)$.

Upon exposure to light, the photocurrent increases significantly, reaching approximately $12 \mu\text{A}$ (Fig. 5c). To further investigate this effect, transient photocurrent measurements were carried out at zero bias using a laser with wavelength of approximately 686 nm (Fig. 5d). Under these conditions, the dark current remains practically negligible, while the photocurrent rises to around $0.35 \mu\text{A}$ upon laser illumination.

To investigate the possible effect of light radiation on EuZn_2P_2 , we performed ESR measurements with 365, 462, 625 nm illumination and, from these spectra, we obtain the angle-dependent $\Delta H(\phi)$ and $\Delta g(\phi)$ under the effect of light.

IV. DISCUSSION

A. Polaron formation

The ESR-derived parameters (Fig. 4) offer insight into the underlying spin dynamics in EuZn_2P_2 . The g -shift Δg , defined as the difference between the experimental value g_{exp} and the expected value for insulating Eu^{2+} (1.993(2)) [38], can be expressed as:

$$\Delta g = J_{fs}\eta(E_F), \quad (6)$$

where J_{fs} is the exchange interaction parameter between Eu^{2+} ions and the s spin carriers, and $\eta(E_F)$ denotes the density of states at the Fermi energy.

Since J_{fs} and Δg are related by Eq. 6, this means that if $\Delta g < 0$ then an AFM polarization of spin carriers is expected, whereas $\Delta g > 0$ indicates FM polarization of spin carriers. The persistent positive Δg across the measured temperature range implies the presence of FM polarization of spin carriers surrounding the Eu^{2+} ions [39]. The observed enhancement of Δg near T_N reinforces the presence of short-range FM correlations, suggesting polaronic formation prior to long-range ordering [35].

Magnetic polarons are quasiparticles formed by charge carriers which couple to the local magnetic moments via exchange interactions [40]. As a result, carriers become localized, and their wave functions are confined by this coupling. The main macroscopic consequence of this phenomenon is an increase in the resistivity [9].

The evolution of ΔH further supports this scenario. Between $70 < T < 200$ K the ΔH narrows. However, as the system approaches T_N , ΔH broadens considerably, likely due to the onset of strong FM magnetic correlations. Such behavior is consistent with previous observations in systems where magnetic polarons emerge as a precursor to collective magnetic ordering [38, 41].

The existence of these localized states is related to an activated type of resistivity ($\rho \sim e^{\frac{\Delta}{k_B T}}$). As T_N is reached, magnetic polarons begin to percolate; this percolation enables carrier transport, which in turn leads to a sharp drop in resistivity. Based on our results, the formation of magnetic polarons in EuZn_2P_2 appears highly plausible. First, we observe a minimum in ΔH around 50 K, which aligns closely with the resistivity peak re-

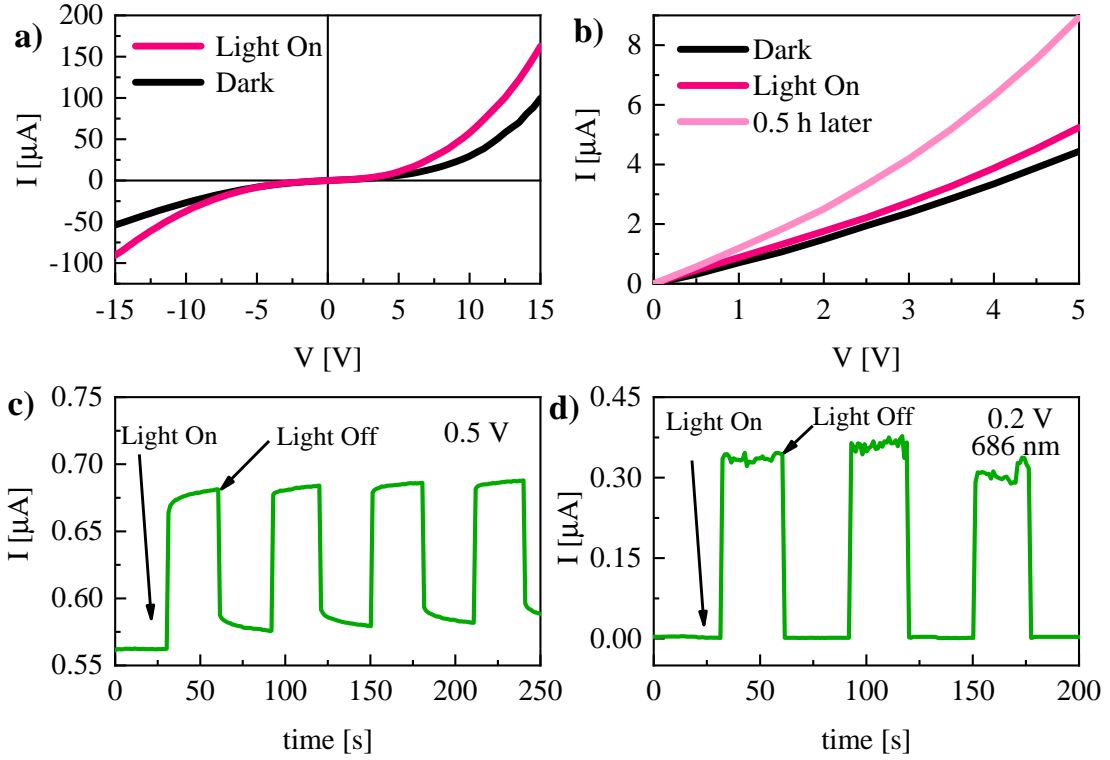


FIG. 5. a) and b) are the $I - V$ curves without (dark) and with (purple) illumination. In d) we observe that the current persists to enhance after 0.5 h. c) Transient curves for 0.5 V and d) for 0 V for a laser with 696 nm wavelength with a $t \sim 30$ s interval between the pulses is approximately.

ported in a previous study [32]. This minimum may be associated with the overlapping phase of magnetic polarons. Second, the evidence from Δg also supports this scenario: the shift in Δg is indicative of spin carrier polarization.

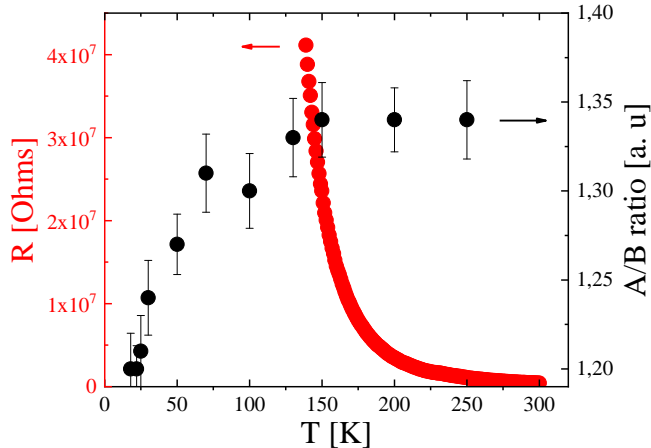


FIG. 6. A/B ratio (dark) and the electrical resistance plot (red). As the system is cooled, the ESR spectra tends to be more symmetric. As a consequence, we expect that the material should have a high insulating regime at low temperatures.

The A/B ratio derived from the ESR line shape re-

veals a clear temperature dependence, becoming more symmetric at lower temperatures as shown in Fig. 6. This trend reflects a transition towards a more insulating state, in agreement with increased resistance, and is indicative of carrier localization [35]. The correlation between ESR symmetry and resistance supports the interpretation of spin carriers being trapped within magnetic polarons, reducing the electrical conduction. These results collectively support a scenario wherein magnetic polarons in EuZn_2P_2 form anisotropically within a three-dimensional spin environment. Although visualized as localized regions, the shape and extent of polarons may vary with magnetic anisotropy and spin dynamics.

With the possibility of magnetic polarons formation already established, we now turn our attention to light-dependent ESR measurements.

B. Photoinduced effects

The $I - V$ and transient response data (Fig. 5) demonstrate a robust photovoltaic effect in EuZn_2P_2 , with measurable increases in the current under visible light excitation. The nonlinear, asymmetric behavior of the $I - V$ curves resembles that of semiconductor photodiodes, suggesting potential utility in optoelectronic applications. To quantitatively assess the performance of EuZn_2P_2 as

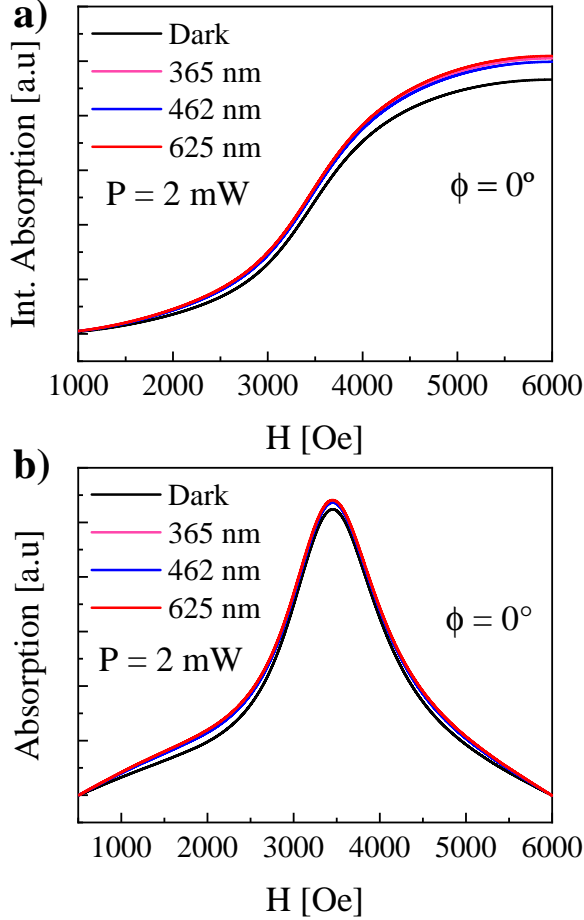


FIG. 7. a) Integrated absorption and b) Absorption spectra for the dark (black), 365 (pink), 462 (blue) and 625 nm (red) for a 2 mW power obtained from the room-temperature ESR spectra.

a photodetector, we must evaluate the key performance parameters: responsivity (R), detectivity (D), and external quantum efficiency (η_{ext}) [42]:

$$R = \frac{I_{photo}}{P}, \quad (7)$$

$$D^* = R \sqrt{\frac{S}{2eI_{dark}}}, \quad (8)$$

$$\eta_{external} = \frac{h\nu I_{photo}}{eP}, \quad (9)$$

where P is the power of the light source, S is the effective surface area, and I_{dark} and I_{photo} are the dark current and the photogenerated electrical current, respectively. For the 686 nm wavelength ($P \approx 92.5$ mW), we obtain $R = 3.78$ A/W, $D = 1.39 \times 10^{11}$ Jones, and $\eta_{external} \approx 6\%$. These values are typical of a material with good

performance as a photodetector, demonstrating potential for applications.

The ESR spectra under light irradiation with wavelengths of 365, 462 and 625 nm were analyzed to investigate the light-induced effects on the ESR spectra (Figs. 7 and 8).

A small broadening of ΔH is readily observed for the ESR spectra under the irradiation of visible light (Fig. 8a). As previously mentioned, such broadening may be indicative of more significant FM correlations. In this context, the light-induced ESR response provides two key insights:

1. Light affects the magnetic behavior (by the ΔH light-induced broadening) of EuZn_2P_2 ;
2. Photoinduced electrons at the surface may play an active role in modulating the ESR signal.

The g -factor, however, does not show any significant variation at least for the g_{\perp} component (Fig. 8b). This negligible change in Δg is likely due to the limited penetration depth of the radiation. Since we use relatively low-energy photons, the light is not able to penetrate deeply into the bulk of the material. As a result, the observed g -value, which primarily reflects the bulk contribution, is only weakly sensitive to changes in the surface region.

The ESR intensity, displayed in Fig. 7a, is directly proportional to the magnetic susceptibility and the population of resonant spins in the material. Thus, an increase in I_{ESR} may indicate an increase in the spin population and/or an enhancement of the magnetic susceptibility. Interestingly, under the effect of light irradiation, we observe a clear increase in ESR intensity. This enhancement may be associated with photoinduced electron production at the surface of EuZn_2P_2 that contributes to the increased signal. This supports the idea that the radiation primarily affects only a few surface layers, but the effect remains readily detectable via ESR.

Altogether, these light-induced effects in EuZn_2P_2 are manifestations of a relevant photomagnetic effect, which describes how the magnetic properties of a material (usually ferromagnetism) respond to light, typically leading to either enhancement or suppression of magnetization [43]. However, this phenomenon is rarely observed in intermetallic compounds and is more commonly reported in organic and molecular magnetic systems [44–48]. Further experimental investigations will be useful to help clarify this effect in EuZn_2P_2 .

V. CONCLUSIONS

We successfully grew high-quality EuZn_2P_2 single crystals using the Sn-flux method. Mössbauer spectroscopy at 300 K shows a single resonance line at negative velocity, confirming the Eu^{2+} oxidation state. Analysis of the Mössbauer spectra reveals that the hyperfine field of Eu

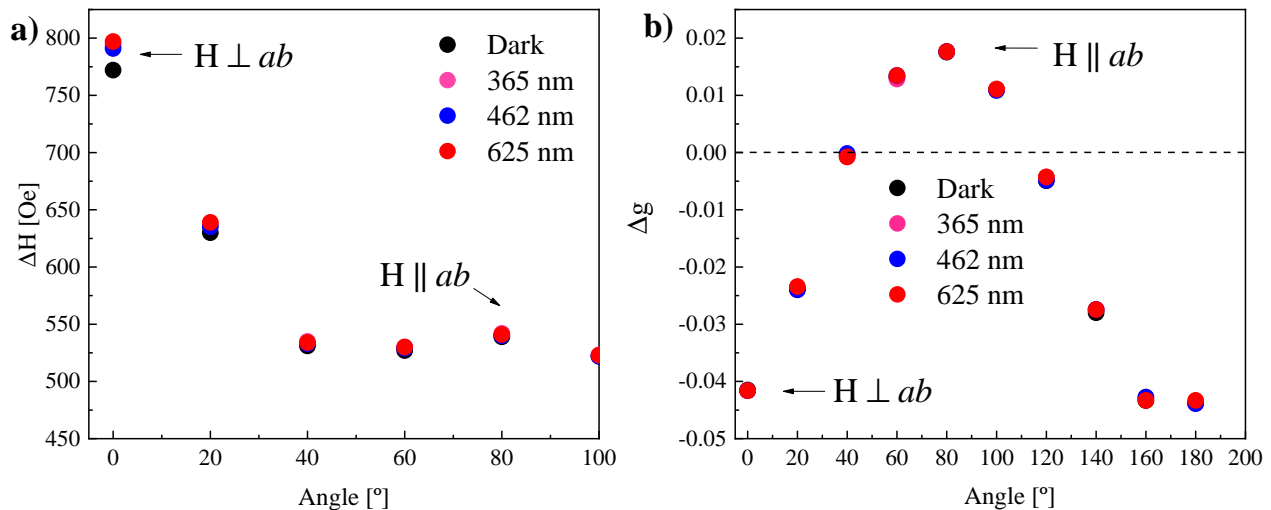


FIG. 8. a) $\Delta H(\phi)$ and b) $\Delta g(\phi)$ without and with radiation. It's possible to observe small changes of the ΔH upon illumination but no significant in the $\Delta g(\phi)$.

ions is canted by $\theta = 46(3)^\circ$ relative to the principal component of the crystal electric field (CEF). ESR measurements demonstrate that the linewidth ΔH in EuZn₂P₂ is dominated by spin-spin interactions and exhibits g -shift $\Delta g > 0$. These shifts are associated with the formation of internal fields caused by electron polarization around Eu²⁺. Such behavior, consistent with the A/B ratio and electrical resistance plot, supports the presence of anisotropic magnetic polarons. Angle-dependent analysis of $\Delta H(\phi)$ indicates that short-wavelength fluctuations are dominated by the C_{3D} parameter, highlighting the three-dimensional nature of magnetic interactions in EuZn₂P₂ with strong interlayer coupling. From the $\Delta g(\phi)$ analysis, we calculated g_{\parallel} and g_{\perp} , finding that FM interactions are stronger along the ab -plane than in the c -axis. Specifically, Δg_{\perp} is positive while Δg_{\parallel} is negative. ESR measurements under illumination show differences compared to dark conditions. The linewidth ΔH broadens with light exposure, suggesting that light influences the magnetization of EuZn₂P₂. Additionally, the ESR intensity increases under illumination, likely due to surface photoinduced electrons. These observations point toward the possibility of a photomagnetic effect in EuZn₂P₂, although further experiments are necessary to confirm and detail its occurrence.

We also discovered a photovoltaic effect with promising performance parameters, characterized by responsivity,

detectivity, and external quantum efficiency. Taken together, magnetic polarons, photomagnetism, and photovoltaic behavior establish EuZn₂P₂ as a compelling platform to study the interplay between magnetism, optics, and electronics, with significant potential for applications in spintronics and quantum technologies.

VI. ACKNOWLEDGMENTS

The authors thanks P. G. Pagliuso and S. Sundar for fruitful discussions. We also thank K. K. F. Barbosa and F. F. Ferreira for the PXRD measurements and the Multiuser Central Facilities at UFABC for the experimental support. We acknowledge the financial support of Brazilian funding agencies CAPES, CNPq (Contracts No. 140921/2022-2, No. 88887.837417/2023-00), FAPESP (No. 2017/20989-8, No. 2017/10581-1). E. Baggio-Saitovitch, J.F. Oliveira, and M.A.V. Heringer thank Fundação Carlos Chagas Filho de Amparo a Pesquisa do Estado do Rio de Janeiro (FAPERJ) for Emeritus and PDN10 fellowships, and also for several grants including E-26/010.002990/2014 and E-26/210.496/2024. M. Cabrera-Baez acknowledges the support of the INCT of Spintronics and Advanced Magnetic Nanostructures (INCT-SpinNanoMag), CNPq 406836/2022-1 and PROPESQI-UFPE.

[1] S. M. Kauzlarich, Zintl phases: From curiosities to impactful materials, *Chemistry of Materials* **35**, 7355 (2023).
 [2] J. Shuai, J. Mao, S. Song, Q. Zhang, G. Chen, and Z. Ren, Recent progress and future challenges on thermoelectric zintl materials, *Materials Today Physics* **1**, 74 (2017).

[3] R. Freer, D. Ekren, T. Ghosh, K. Biswas, P. Qiu, S. Wan, L. Chen, S. Han, C. Fu, T. Zhu, *et al.*, Key properties of inorganic thermoelectric materials—tables (version 1), *Journal of Physics: Energy* **4**, 022002 (2022).
 [4] J. H. Westbrook and R. L. Fleischer, *Intermetallic compounds: principles and practice*, (No Title) (1995).

- [5] Z.-C. Wang, J. D. Rogers, X. Yao, R. Nichols, K. Atay, B. Xu, J. Franklin, I. Sochnikov, P. J. Ryan, D. Haskell, *et al.*, Colossal magnetoresistance without mixed valence in a layered phosphide crystal, *Advanced Materials* **33**, 2005755 (2021).
- [6] J.-Z. Ma, S. Nie, C. Yi, J. Jandke, T. Shang, M.-Y. Yao, M. Naamneh, L. Yan, Y. Sun, A. Chikina, *et al.*, Spin fluctuation induced weyl semimetal state in the paramagnetic phase of EuCd_2As_2 , *Science advances* **5**, eaaw4718 (2019).
- [7] S. Luo, Y. Xu, F. Du, L. Yang, Y. Chen, C. Cao, Y. Song, and H. Yuan, Colossal magnetoresistance and topological phase transition in EuZn_2As_2 , *Physical Review B* **108**, 205140 (2023).
- [8] F. Du, L. Yang, Z. Nie, N. Wu, Y. Li, S. Luo, Y. Chen, D. Su, M. Smidman, Y. Shi, *et al.*, Consecutive topological phase transitions and colossal magnetoresistance in a magnetic topological semimetal, *npj Quantum Materials* **7**, 65 (2022).
- [9] P. Littlewood, Transport and magnetoresistance in low carrier density ferromagnets, *Acta Physica Polonica A* **97**, 7 (2000).
- [10] H. Zhang, F. Du, X. Zheng, S. Luo, Y. Wu, H. Zheng, S. Cui, Z. Sun, Z. Liu, D. Shen, *et al.*, Electronic band reconstruction across the insulator-metal transition in colossally magnetoresistive EuCd_2P_2 , *Physical Review B* **108**, L241115 (2023).
- [11] V. Sunko, Y. Sun, M. Vranas, C. C. Homes, C. Lee, E. Donoway, Z.-C. Wang, S. Balguri, M. B. Mahendru, A. Ruiz, *et al.*, Spin-carrier coupling induced ferromagnetism and giant resistivity peak in EuCd_2P_2 , *Physical Review B* **107**, 144404 (2023).
- [12] E. Heinrich, T. Posske, and B. Flebus, Topological magnetic phase transition in Eu-based A-type antiferromagnets, *Physical Review B* **106**, 214402 (2022).
- [13] D. J. Marsh, K. C. Fong, E. W. Lentz, L. Šmejkal, and M. N. Ali, Proposal to detect dark matter using axionic topological antiferromagnets, *Physical Review Letters* **123**, 121601 (2019).
- [14] K. Ishiwata and K. Nomura, Collective excitations in magnetic topological insulators and axion dark matter search, *arXiv preprint arXiv:2406.09705* (2024).
- [15] J. Schütte-Engel, D. J. Marsh, A. J. Millar, A. Sekine, F. Chadha-Day, S. Hoof, M. N. Ali, K. C. Fong, E. Hardy, and L. Šmejkal, Axion quasiparticles for axion dark matter detection, *Journal of Cosmology and Astroparticle Physics* **2021** (08), 066.
- [16] A. Sekine and K. Nomura, Axion electrodynamics in topological materials, *Journal of Applied Physics* **129** (2021).
- [17] M. Manzoor, D. Behera, R. Sharma, M. W. Iqbal, S. Mukherjee, R. Khenata, S. Bin-Omran, T. Alshahrani, E. El Shiekh, and T. Ouahrani, Structural, electronic, optical, and thermoelectric studies on zintl SrCd_2Pn_2 ($\text{Pn} = \text{P/As}$) compounds for solar cell applications: A first principle approach, *Journal of Solid State Chemistry* **326**, 124188 (2023).
- [18] Z. Yuan, D. Dahliah, M. R. Hasan, G. Kassa, A. Pike, S. Quadir, R. Claes, C. Chandler, Y. Xiong, V. Kyveryga, *et al.*, Discovery of the zintl-phosphide BaCd_2P_2 as a long carrier lifetime and stable solar absorber, *Joule* **8**, 1412 (2024).
- [19] G. Souadi, First principles investigations of optoelectronic and thermoelectric properties of novel BaMg_2X_2 ($\text{X} = \text{P, As, Sb}$) alloys for renewable energy applications, *Inorganic Chemistry Communications*, 112768 (2024).
- [20] A. Khireddine, A. Bouhemadou, S. Maabed, S. Bin-Omran, R. Khenata, and Y. Al-Douri, Elastic, electronic, optical and thermoelectric properties of the novel zintl-phase Ba_2ZnP_2 , *Solid State Sciences* **128**, 106893 (2022).
- [21] T. Amin, A. H. Reshak, Z. Zada, I. ur Rahman, D. Ali, A. M. Khan, A. Laref, M. M. Ramli, *et al.*, Structural, opto-electronic and transport properties of zintl compound YbZn_2Y_2 ($\text{Y} = \text{P, As, Sb, Bi}$), *Engineered Science* **31**, 1258 (2024).
- [22] A. Kirilyuk, A. V. Kimel, and T. Rasing, Ultrafast optical manipulation of magnetic order, *Reviews of Modern Physics* **82**, 2731 (2010).
- [23] A. Kabychenkov, Magnetic phase transitions in a light wave, *Sov. Phys. JETP* **73**, 672 (1991).
- [24] A. Kimel, A. Kirilyuk, P. Usachev, R. Pisarev, A. Balbashov, and T. Rasing, Ultrafast non-thermal control of magnetization by instantaneous photomagnetic pulses, *Nature* **435**, 655 (2005).
- [25] V. Dobrovolsky and V. Rossokhaty, Planar photomagnetic effect soi sensors for various applications with low detection limit, in *Science and Technology of Semiconductor-On-Insulator Structures and Devices Operating in a Harsh Environment: Proceedings of the NATO Advanced Research Workshop on Science and Technology of Semiconductor-On-Insulator Structures and Devices Operating in a Harsh Environment Kiev, Ukraine 26–30 April 2004* (Springer, 2005) pp. 303–308.
- [26] G. Barrera, D. Martella, F. Celegato, N. Fuochi, M. Coisson, C. Parmeggiani, D. S. Wiersma, and P. Tiberio, Light-controlled magnetic properties: An energy-efficient opto-mechanical control over magnetic films by liquid crystalline networks, *Advanced Science* **11**, 2408273 (2024).
- [27] A. V. Kimel and M. Li, Writing magnetic memory with ultrashort light pulses, *Nature Reviews Materials* **4**, 189 (2019).
- [28] B. H. Toby and R. B. Von Dreele, Gsas-ii: the genesis of a modern open-source all purpose crystallography software package, *Journal of Applied Crystallography* **46**, 544 (2013).
- [29] T. Berry, V. J. Stewart, B. W. Redemann, C. Lygouras, N. Varnava, D. Vanderbilt, and T. M. McQueen, Dipolar magnetic interactions and A-type antiferromagnetic order in the zintl phase insulator EuZn_2P_2 , *arXiv preprint arXiv:2203.12739* (2022).
- [30] F. Grandjean and G. J. Long, Mössbauer spectroscopy of europium-containing compounds, in *Mössbauer Spectroscopy Applied to Inorganic Chemistry* (Springer, 1989) pp. 513–597.
- [31] M. A. Ahmida *et al.*, Theoretical review of mössbauer effect, hyperfine interactions parameters and the valence fluctuations in eu systems, *Journal of Applied Mathematics and Physics* **7**, 254 (2019).
- [32] D. Rybicki, K. Komędera, J. Przewoźnik, L. Gondek, C. Kapusta, K. Podgórska, W. Tabiś, J. Żukrowski, L. M. Tran, M. Babij, *et al.*, Ambient-and high-pressure studies of structural, electronic, and magnetic properties of single-crystal EuZn_2P_2 , *Physical Review B* **110**, 014421 (2024).

- [33] P. F. S. Rosa, W. Iwamoto, L. Holanda, R. Ribeiro, P. Pagliuso, C. Rettori, and M. Avila, Magnetic polaron effect in $\text{Sr}_{8-x}\text{Eu}_x\text{Ga}_{16}\text{Ge}_{30}$ clathrates probed by electron spin resonance, *Physical Review B—Condensed Matter and Materials Physics* **87**, 224414 (2013).
- [34] M. Cabrera-Baez, A. Naranjo-Urbe, J. Osorio-Guillén, C. Rettori, and M. Avila, Multiband electronic characterization of the complex intermetallic cage system $\text{Y}_{1-x}\text{Gd}_x\text{Co}_2\text{Zn}_2\text{O}$, *Physical Review B* **92**, 214414 (2015).
- [35] M. S. Cook, E. A. Peterson, C. S. Kengle, E. Kennedy, J. Sheeran, C. Girod, G. Freitas, S. M. Greer, P. Abbamonte, P. Pagliuso, *et al.*, Magnetic polaron formation in EuZn_2P_2 , arXiv preprint arXiv:2504.05494 (2025).
- [36] J. Sichelschmidt, P. Chaillouleau, S. Krebber, A. E. Mard, C. Krellner, and K. Kliemt, Electron spin resonance of eu on triangular layers in EuT_2P_2 ($T = \text{Mn, Zn, Cd}$), arXiv preprint arXiv:2505.06060 (2025).
- [37] D. Nikolic, A. Vasic, I. Fetahovic, K. Stankovic, and P. Osmokrovic, Photodiode behavior in radiation environment, *Scientific Publications of the State University of Novi Pazar Series A* **3**, 27 (2011).
- [38] P. Rosa, C. Adriano, T. Garitezi, R. Ribeiro, Z. Fisk, and P. Pagliuso, Electron spin resonance of the intermetallic antiferromagnet EuIn_2As_2 , *Physical Review B—Condensed Matter and Materials Physics* **86**, 094408 (2012).
- [39] A. Abragam and B. Bleaney, *Electron Paramagnetic Resonance of Transition Ions*, International series of monographs on physics (Clarendon P., 1970).
- [40] D. R. Yakovlev and W. Ossau, Magnetic polarons, in *Introduction to the physics of diluted magnetic semiconductors* (Springer, 2010) pp. 221–262.
- [41] J. C. Souza, S. Thomas, E. Bauer, J. Thompson, F. Ronning, P. Pagliuso, and P. Rosa, Microscopic probe of magnetic polarons in antiferromagnetic $\text{Eu}_5\text{In}_2\text{Sb}_6$, *Physical Review B* **105**, 035135 (2022).
- [42] M. Yang, H. Zhou, and J. Wang, Topological insulators photodetectors: Preparation, advances and application challenges, *Materials Today Communications* **33**, 104190 (2022).
- [43] U. Enz, W. Lems, R. Metselaar, P. Rijnierse, and R. Teale, Photomagnetic effects, *IEEE Transactions on Magnetics* **5**, 467 (1969).
- [44] D. Garnier, J.-R. Jiménez, Y. Li, J. Von Bardeleben, Y. Journaux, T. Augenstein, E. Moos, M. Gamer, F. Breher, and R. Lescouëzec, $K \subset [\text{Fe}^{II}(\text{Tp})(\text{CN})_3]_4[\text{Co}^{III}(\text{p}^z\text{Tp})]_3[\text{Co}^{II}(\text{p}^z\text{Tp})]$: a neutral soluble model complex of photomagnetic prussian blue analogues, *Chemical science* **7**, 4825 (2016).
- [45] J. M. Herrera, V. Marvaud, M. Verdaguer, J. Marrot, M. Kalisz, and C. Mathoniere, Reversible photoinduced magnetic properties in the heptanuclear complex $[\text{Mo}^{IV}(\text{CN})_2(\text{CN}-\text{CuL})_6]^{8+}$: A Photomagnetic High-Spin Molecule, *Angewandte Chemie International Edition* **43**, 5468 (2004).
- [46] C. J. O'Connor *et al.*, Electric, magnetic, and photomagnetic properties of the amorphous metallic spin-glass $\text{Ni}_3(\text{SbTe}_3)_2$, *Journal of Materials Chemistry* **2**, 829 (1992).
- [47] B. Wu, L. Ren, C. J. O'Connor, J. Tang, J.-S. Jung, J. Ferré, and J.-P. Jamet, Photo-induced magnetic behavior in the amorphous spin-glass material $\text{Co}_3(\text{SbTe}_3)_2$, *Journal of materials research* **9**, 909 (1994).
- [48] C. J. O'Connor and J. F. Noonan, Photo-induced magnetic bubbles in the spin glass alloy Fe_2SnTe_4 , *Journal of Physics and Chemistry of Solids* **48**, 303 (1987).
- [49] X. Chen, W. Yang, J.-Y. Lu, Z. Zhou, Z. Ren, G.-H. Cao, S. Dong, and Z.-C. Wang, Carrier-induced transition from antiferromagnetic insulator to ferromagnetic metal in the layered phosphide EuZn_2P_2 , *Physical Review B* **109**, L180410 (2024).
- [50] S. Krebber, M. Kopp, C. Garg, K. Kummer, J. Sichelschmidt, S. Schulz, G. Poelchen, M. Mende, K. Warawa, M. D. Thomson, *et al.*, Colossal magnetoresistance in EuZn_2P_2 and its electronic and magnetic structure, arXiv preprint arXiv:2302.14539 (2023).
- [51] Z. Yang, X. Bao, S. Tan, and Y. Zhang, Magnetic polaron conduction in the colossal magnetoresistance material $\text{Fe}_{1-x}\text{Cd}_x\text{Cr}_2\text{S}_4$, *Physical Review B* **69**, 144407 (2004).
- [52] J. Ying, L. Tang, F. Chen, X. Chen, and V. V. Struzhkin, Coexistence of metallic and insulating channels in compressed YbB_6 , *Physical Review B* **97**, 121101 (2018).
- [53] L. Li, K. Sun, C. Kurdak, and J. Allen, Emergent mystery in the kondo insulator samarium hexaboride, *Nature Reviews Physics* **2**, 463 (2020).
- [54] D. Y. Usachov, S. Krebber, K. A. Bokai, A. V. Tarasov, M. Kopp, C. Garg, A. Virovets, J. Müller, M. Mende, G. Poelchen, *et al.*, Magnetism, heat capacity, and electronic structure of EuCd_2P_2 in view of its colossal magnetoresistance, *Physical Review B* **109**, 104421 (2024).
- [55] P. Rosa, Y. Xu, M. Rahn, J. Souza, S. Kushwaha, L. Veiga, A. Bombardi, S. Thomas, M. Janoschek, E. Bauer, *et al.*, Colossal magnetoresistance in a non-symmorphic antiferromagnetic insulator, *npj Quantum Materials* **5**, 52 (2020).
- [56] G. Feher and A. Kip, Electron spin resonance absorption in metals. i. experimental, *Physical Review* **98**, 337 (1955).
- [57] K. C. Kao, *Dielectric phenomena in solids* (Elsevier, 2004).
- [58] S. R. Goldman, K. Kalikstein, and B. Kramer, Dember-effect theory, *Journal of Applied Physics* **49**, 2849 (1978).
- [59] K. Kugel, A. Rakhmanov, A. Sboychakov, M. Y. Kagan, and S. Ogarkov, The structure of magnetic polarons in doped antiferromagnetic insulators, *Physica B: Condensed Matter* **403**, 1353 (2008).
- [60] A. Abragam and B. Bleaney, *Electron paramagnetic resonance of transition ions* (OUP Oxford, 2012).
- [61] S. Ghosh, C. Lane, F. Ronning, E. D. Bauer, J. D. Thompson, J.-X. Zhu, P. Rosa, and S. M. Thomas, Colossal piezoresistance in narrow-gap $\text{Eu}_5\text{In}_2\text{Sb}_6$, *Physical Review B* **106**, 045110 (2022).
- [62] P. Majumdar and P. Littlewood, Magnetoresistance in mn pyrochlore: electrical transport in a low carrier density ferromagnet, *Physical review letters* **81**, 1314 (1998).
- [63] Y. Xu, Z. Song, Z. Wang, H. Weng, and X. Dai, Higher-order topology of the axion insulator EuIn_2As_2 , *Physical review letters* **122**, 256402 (2019).
- [64] K. Singh, S. Dan, A. Ptok, T. Zaleski, O. Pavlosiuk, P. Wiśniewski, and D. Kaczorowski, Superexchange interaction in insulating EuZn_2P_2 , *Physical Review B* **108**, 054402 (2023).
- [65] G. M. Pierantozzi, A. De Vita, C. Bigi, X. Gui, H.-J. Tien, D. Mondal, F. Mazzola, J. Fujii, I. Vobornik, G. Vinai, *et al.*, Evidence of magnetism-induced topological protection in the axion insulator candidate EuSn_2P_2 ,

- Proceedings of the National Academy of Sciences **119**, e2116575119 (2022).
- [66] S. X. Riberolles, T. V. Trevisan, B. Kuthanazhi, T. Heitmann, F. Ye, D. Johnston, S. Bud'ko, D. Ryan, P. Canfield, A. Kreyssig, *et al.*, Magnetic crystalline-symmetry-protected axion electrodynamics and field-tunable unpinned dirac cones in EuIn_2As_2 , *Nature communications* **12**, 999 (2021).
- [67] M. Hennion, F. Moussa, G. Biotteau, J. Rodriguez-Carvajal, L. Pinsard, and A. Revcolevschi, Evidence of anisotropic magnetic polarons in $\text{La}_{0.94}\text{Sr}_{0.06}\text{MnO}_3$ by neutron scattering and comparison with Ca-doped magnetites, *Physical Review B* **61**, 9513 (2000).
- [68] L. J. de Jongh, *Magnetic properties of layered transition metal compounds*, Vol. 9 (Springer Science & Business Media, 2012).
- [69] P. M. Richards and M. Salamon, Exchange narrowing of electron spin resonance in a two-dimensional system, *Physical Review B* **9**, 32 (1974).
- [70] W. Xin, X.-K. Li, X.-L. He, B.-W. Su, X.-Q. Jiang, K.-X. Huang, X.-F. Zhou, Z.-B. Liu, and J.-G. Tian, Black-phosphorus-based orientation-induced diodes, *Advanced Materials* **30**, 1704653 (2018).